Volume 1 | Number 1 | Jan 2013 | Pages 1–100

Journal of
Materials Chemistry A

Materials for energy and sustainability
www.rsc.org/materialsA

Li⁺

ROYAL SOCIETY
OF CHEMISTRY

ROYAL SOCIETY
OF **CHEMISTRY**

www.rsc.org/materialsA

Journal Name

COMMUNICATION

Exploring the potential of polymer battery cathodes with electrically conductive molecular backbone

Alexandru Vlad[1,2*], Kevin Arnould[2], Bruno Ernould[2], Louis Sieuw[2], Julien Rolland[2] and Jean-François Gohy[2]

[1]Institute of Information and Communication Technologies, Electronics and Applied Mathematics, Electrical Engineering, and [2]Institute of Condensed Matter and Nanosciences, Bio- and Soft Matter, Université catholique de Louvain, Louvain-la-Neuve, B-1348 Belgium.

Corresponding Author: alexandru.vlad@uclouvain.be

Organic redox materials have the potential to radically shift the battery technology landscape. Here, the chemical synthesis of poly(2,5-dihydroxyaniline) with intrinsic electrical conduction and a theoretical energy storage capacity of 443 mAh/g is detailed for the first time. The genuine intramolecular cross-hybridization of quinone redox and polyaniline conductor moieties leads to a subtle interplay between redox stability and the lithiation capacity with the underlying processes being discussed. Superior to the conventional electrode materials performances are expected upon further optimization of this novel class of organic mixed ion and electron conductors for energy storage.

Organic battery materials are regarded as a potential solution for a sustainable energy future.[1-4] Being still under development, this technology moreover offers broad possibilities with respect to the chemical tuning of the redox potential, number of electron exchanged *per* molecule unit (i.e. specific charge storage capacity) as well as easier compatibility with other than lithium chemistries including sodium, magnesium and polymer-air batteries.[5-10]

The requirements for an organic material to be suitable as a battery electrode are: (i) reversible redox process; (ii) low molar mass accompanied by a multi-electron exchange process, preferentially; (iii) limited or no solubility to avoid elution of the active material from the electrode (yet, adequate swelling is preferred to enable efficient ion transport) in battery electrolytes; (iv) finite electrical conductivity for efficient charge collection; and (v) simple materials and synthesis approaches. Merging all these characteristics within a single material seems rather difficult and many of the studied organic materials so far fail to comply with all these requirements at the same time.[11]

The carbonyl reversible redox process has been intensely studied over the past years, with the quinone - hydroquinone based molecular structures being the most representative example.[12-14] This low molar mass couple undergoes a reversible two-electron exchange process at a relatively high potential (average of 2.6 V vs. Li/Li$^+$) resulting in very appealing characteristics: theoretical specific capacity of 495 mAh/g corresponding to an energy density above 1.2 kWh/kg. Unfortunately, pure quinones hardly satisfy the above listed requirements. Many approaches have been thus developed over the past years to render this class of materials battery relevant including solid-state cells,[15,16] use of high surface area host materials for efficient physisorption[17-19] as well as surface and molecular grafting immobilization approaches.[20,21]

Simple polyquinone molecular formulations are of particular interest because they maintain the high specific capacity and can limit to a certain extent the solubility.[22-24] For example, halogenated polyquinone oligomers were originally proposed by Foos[25] and latter developments detailed on the use of poly(2,5-dihydroxy-1,4-benzoquinone-3,6-methylene) as active material for lithium batteries with promising performances.[26] However, probably due to the limited electrical conductivity, finite solubility as well as partial material utilization, underestimated performances were attained (about 20 to 35% of the theoretical capacity was accessed at the first cycle). Recently, poly(quinone-sulfide) was synthesized and successfully applied as a positive electrode battery material and shown to have excellent performances. Nonetheless, the specific capacity was penalized by the large molar mass and no details were provided regarding the electrical conduction properties of poly(quinone-sulfides).[27] Although excellent advances have been provided to date, there is large room for further improvements.[13]
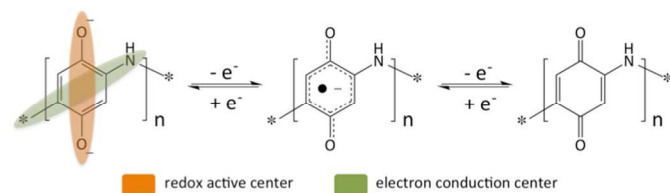
Scheme 1. Molecular formula of poly(2,5-dihydroxyaniline) and the redox mechanism based for a two-electron per monomer unit process resulting in a theoretical capacity of 443 mAh/g. Due to the genuine chemical design, PDHA hybridizes the redox properties of quinone groups, which are part of the polymer backbone, with the electrical conduction of π-conjugation in polyaniline.

In this work, we detail for the first time the two-step chemical synthesis and battery use of poly(2,5-dihydroxyaniline) (PDHA). The active redox material is obtained by chemical de-methylation of poly(2,5-dimethoxyaniline) (PDMA). This is different from previous electrochemical attempts to synthesize PDHA from PDMA and results in a considerably enhanced electrochemical response due to a much higher demethylation yield.[28,29] Due to its genuine chemical design, PDHA hybridizes the redox properties of quinone groups, which are part of the polymer backbone, with the electrical conduction of π-conjugation in polyaniline (Scheme 1). Although resembling structures have been proposed in the past, there are major conceptual differences with our approach.[25,30] Indeed, by using a naphtoquinone-based polymer, both functions were molecularly decoupled and the molar mass increased.[26] Although not specifically investigated nor mentioned, the poly-naphtoquinone could be considered as well as an electric conductor with potentially limited solubility in organic electrolytes. Recently, a naphthalene-dicarboximide-bithiophene based redox conducting polymer was also proposed and shown to support fast electrode kinetics.[31] Interestingly, in an analogous study, the quinone redox kinetics in thin films of electropolymerized poly(pyrrol-3-ylhydroquinone) was found to be the limiting step, rather than the electron transport through the polypyrrole conducting backbone.[32] As we will show next, poly(2,5-dihydroxyaniline) holds near-to-ideal organic battery electrode properties, i.e. satisfies all of the above-mentioned prerequisites. Although full material utilization was found to limit the cycling performances, the underlying mechanism is comprehensibly detailed and guidelines for further developments are provided.
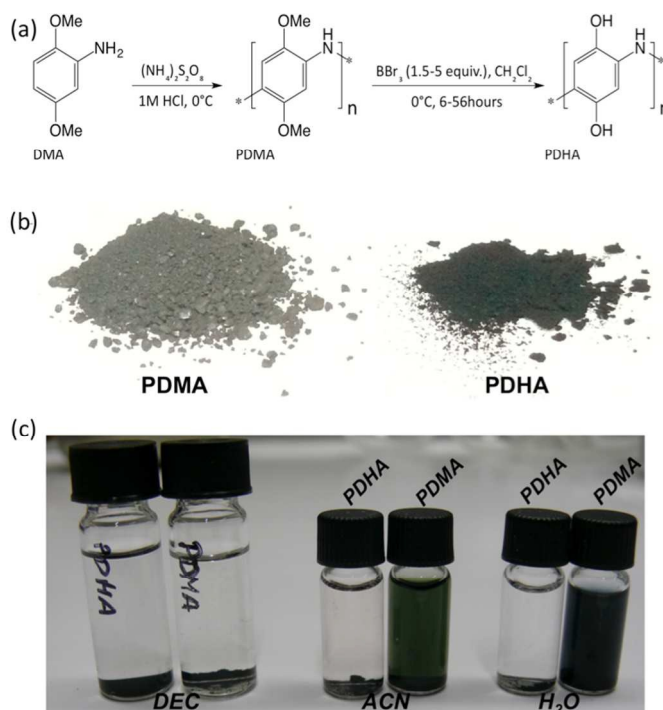

Figure 1. (a) Applied route for PDMA and PDHA synthesis. (b) Optical photographs of the synthesized powders. PDHA has a darker green appearance (acid doped forms). (c) Solubility tests in diethyl carbonate, acetonitrile and deionized water.

The two-step chemical synthesis route adopted in this work is summarized in Figure 1a (details are provided in Supporting Information). Oxidative polymerization of 2,5-dimethoxyaniline was adopted to allow for gram-scale synthesis.[33] For the second step, the BBr_3 assisted demethylation was preferred due to limited side-effects, especially with respect to the degradation of the polyaniline chain.[34] The obtained product has a solid consistency with a dark-green colour (Figure 1b). The dissolution tests showed that PDHA has a much lower solubility than starting PDMA, with reduced solubility in typical battery electrolyte constituents (Figure 1c and Supporting Information).

Several PDHA samples, differing by the demethylation yield were prepared and analysed, with three representative examples (referred to as PDHA$_{1-3}$) discussed here (see Supporting Information for experimental details and more demethylated products, Scheme S1). Table 1 summarizes the elemental analysis results for starting PDMA and obtained PDHA$_{1-3}$ materials. The observed C/N atomic ratio decrease is assigned to an increase in the demethylation yield. Given the elemental analysis errors as well as the presence of possible organic contaminations, precise chemical composition was difficult to assess. The end-series member (PDHA$_3$) could be nevertheless considered as close to totally demethylated.

Material	Composition (wt.%)			Composition (C/N atomic ratio)	Theoretical Formula (C/N atomic ratio)
	C	N	H		
PDMA	57,11	7,34	5,22	9,08	$C_8H_9NO_2$ - (8)
PDHA$_1$	53,25	6,91	4,93	8,99	$C_6H_5NO_2$ - (6)
PDHA$_2$	57,52	8,54	4,46	7,85	$C_6H_5NO_2$ - (6)
PDHA$_3$	54,23	10,16	3,92	6,22	$C_6H_5NO_2$ - (6)

Table 1. Mass elemental analysis of PDMA and three different PDHA materials. From PDHA$_1$ to PDHA$_3$ de-methylation extent increases as evidenced by a decreased C/N atomic ratio.

Next, we entailed structural and chemical analysis of the synthesized materials on the basis of an arsenal of characterization techniques (Figure 2 and Supporting Information Figures S2 - S4). Panels 2a and 2b display Raman and FTIR spectra of PDMA and PDHA$_3$. Raman spectroscopy shows little changes between the two materials, with main characteristics being the decrease of the peaks intensity and the disappearance of the satellite peaks at 1200, 1400 and 1560 cm^{-1} in PDHA. In turn, FTIR provides more insight into structural changes. The two peaks around 1500 cm^{-1} corresponding to the benzenoid and quinonoid forms are preserved in PDHA. Their small shift is attributed to the structural changes accompanying the conversion of PDMA into PDHA. The peaks at 2828 cm^{-1} and 2930 cm^{-1}, characteristic of methoxy group have decreased in intensity and a new broad band at 3200 cm^{-1} characteristic of phenol stretching vibration has appeared. Altogether, compositional and structural analyses (see also Supporting Information, Figures S2 - S4 for X-ray diffraction, thermogravimetric and X-ray photoelectron spectroscopy data) confirm the selective BBr$_3$ assisted demethylation with little structural degradation or scission of the polyaniline chain.

In turn, UV/vis spectroscopy and electrical conductivity measurements revealed the fine structural modifications (Figures 2c and 2d). Acid doped PDMA shows the specific absorption peaks of polyaniline (emeraldine salt form) with the 344 nm peak corresponding to $\pi - \pi^*$ band gap transition, while the 443 nm and >800 nm maxima are due to the presence of the polaron band.[35] These features disappear in the basified form with the peak centered at 600 nm indicative of the exciton band. PDHA maintains the acid doping characteristics with clear optical signature changes between the acidified and basified forms. Nonetheless, the acid doped form of PDHA shows no absorption above 800 nm whereas the 344 nm and 443 nm bands are preserved. All in all, the absorption spectrum of acid doped PDHA contains features of both, emeraldine base and acid forms whereas un-doped forms of PDMA and PDHA have identical features. This is assigned to interrupted π-conjugation of the emeraldine chain (the possible degradation pathways are detailed in Supporting Information, Scheme S2). Finally, conductivity measurements confirmed that PDHA partially preserves the electrical conductivity of the emeraldine, with characteristic acid-base doping / un-doping behaviour (Figure 2d). Consistent with the literature, conductivity of 1M HCl doped PDMA was of ~ 1 S/cm[33] with one order of magnitude loss in conductivity accompanying the demethylation, further confirming the partial π-conjugation degradation.
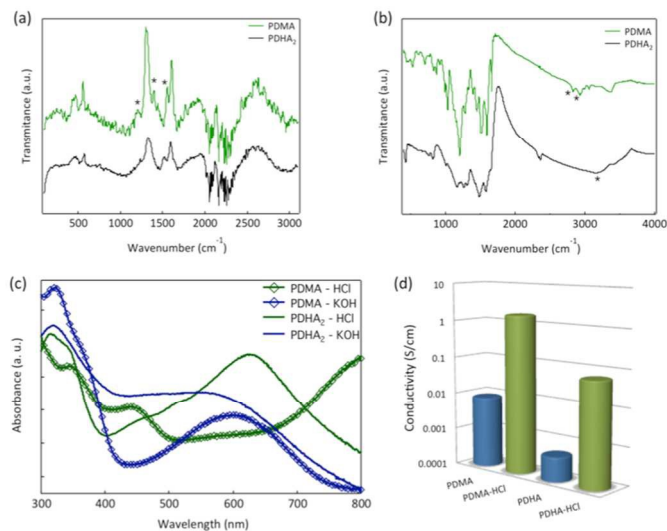

Figure 2. Characterization of the synthesized materials. Characteristic (a) Raman and (b) FTIR spectra of PDMA and PDHA. Stars highlight the major changes detected. (c) UV/vis absorption spectra of PDMA and PDHA in both acidified and basified forms. (d) Electrical conductivity of PDMA and PDHA in the acidified and basified forms.

We next studied the redox properties of the synthesized materials in half-cell configuration using metallic lithium as reference and counter electrode, and organic carbonate based electrolyte. The constant current charge - discharge plots of PDMA and PDHA$_{1-3}$ are shown in Figure 3a and the associated capacity retention versus cycle number are shown in Figure 3b. Pristine PDMA based electrodes have a nominal capacity of about 60 mAh/g whereas PDHA$_1$, PDHA$_2$ and PDHA$_3$ display initial capacities of 120, 180 and 270 mAh/g, respectively. Up to 400% capacity enhancement upon chemical demethylation is attained further evidencing that the chemical approach is more appropriate than the electrochemical route.[29]

The complex interplay between the molecular structure and the electrochemical properties of PDMA and PDHA$_{1-3}$ was analysed and is detailed in the following. First, when corroborating the electrochemical performances with the physico-chemical characteristics, an interesting trend is delineated. The increased extent of demethylation (Table 1) results in (i) solubility decrease, (ii) higher de/lithiation capacity yet, (iii) lower electrochemical cycling stability (Figure 3b).
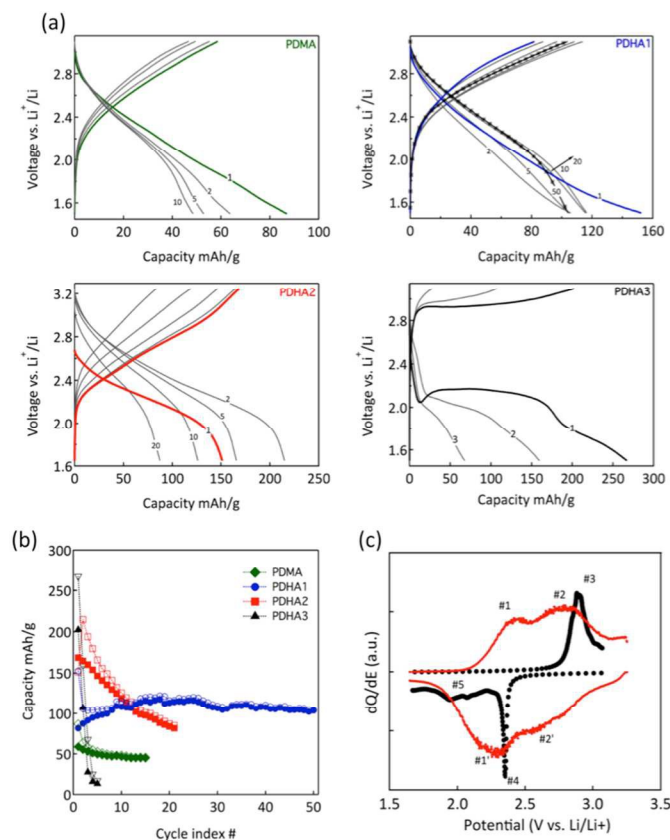
Figure 3. Electrochemical characterization. (a) Constant current charge-discharge (at C/10 rate) profiles for PDMA and PDHA$_{1-3}$. (b) Capacity retention plots of the respective materials. (c) Differential capacity plots for PDHA$_2$ and PDHA$_3$. The characteristic redox peaks are highlighted.

Next, the as-assembled half-cells had generally an open circuit potential in the range of 2.8 - 3.2 V (vs. Li/Li$^+$), requiring first a cathodic activation step. Unexpected, as the direct demethylated product (Figure 1a) is in the reduced form. This signifies that the product is air-sensitive and oxidized during material handling and electrode processing, as already observed in quinone derivatives.[36] It should be also noted that only PDHA$_2$ and PDHA$_3$ display first cycle distinct discharge plateaus. The redox processes are better visualized in the differential capacity plots (Figure 3c). PDHA$_2$ displays a pair of redox peaks centered at 2.3 V (marked with #1 and #1') and 2.6V (marked with #2 and #2') that could be assigned to the two-electron process in PDHA (Scheme 1). PDHA$_3$ shows a strong cathodic peak (#4) followed by a less pronounced response (#5) and only one anodic peak was observed (#3) with subsequent rapid degradation (see further discussion and Supporting Information, Scheme S2).

Finally, it is worth to pay attention to the continuous evolution in the electrochemical response of the analysed PDMA and PDHA$_1$ electrodes. The first discharge is free of any characteristic features whereas subsequent cycling leads to the progressive appearance of a discharge plateau (for instance, cycle 1 vs. cycle 10 for PDMA, Figure 3a; see also Supporting Information - Figure S5 for differential capacity plots of PDMA and PDHA$_1$). The appearance of

the redox plateau for PDHA$_1$ is also accompanied by an increase of the working potential (see for example cycle 50, dotted line in Figure 3a - PDHA$_1$). All in all, the electrochemical responses of PDMA, PDHA$_1$ and PDHA$_2$ look alike after few charge - discharge cycles. We assign this to the progressive in-situ electrochemical conversion (demethylation) of PDMA to PDHA.

From all these observations, a unified redox cycling mechanism is proposed. The major degradation pathway is assigned to the irreversible keto-enol tautomerism of the hydroxyl groups attached to the quinonoids groups of the PDHA chain (Supporting Information, Scheme 2). In fact, such degradation occurs as soon as the demethylation is initiated by de-protecting the methoxy groups of the imine rings (leading as well to the degradation of the π-conjugation, as evidenced by UV/vis and electrical conductivity analysis). To test this, the fully reduced state of PDMA (leucoemeraldine form) was processed and resulted in higher lithiation capacities (Supporting Information, Scheme 1). Furthermore, lower cycling stability in the PDHA$_{1-3}$ series (during the synthesis but also upon electrochemical cycling) is also attributed to the structural transformations in PDHA during the electrochemical cycling. The redox reaction of the polyaniline chain (leucoemeraldine - emeraldine couple, Supporting Information, Scheme S2) leads to the transformation of phenylene into imine rings. Such configurations are unstable due to the keto-enolization that will irreversibly degrade the quinone redox center. Electrochemically induced morphological degradation is expected to play a minor role here[37] since the material adopts an electrolyte swelled amorphous morphology (Figure S2). The development of molecular architectures that will selectively allow a reversible redox process only of the quinone unit is thus of great interest for this emerging organic battery materials family.

Conclusions

To summarize, this work describes the chemical synthesis of poly(2,5-dihydroxyaniline), a cross-hybrid molecular architecture of redox quinone and electron conductive polyaniline. The material holds great potential as an active component for lithium batteries due to its high theoretical specific capacity, electrical conductivity as well as insolubility in common electrolytes. We envisage that further studies of such materials will afford a clearer understanding of the effect of the chemical structure on the electrochemical performances as well as full material utilization based on a two-electron process and stable cycling.

Electronic Supplementary Information (ESI) available.

1. M. Armand and J. M. Tarascon, *Nature*, 2008, **451**, 652–657.
2. H. Chen, M. Armand, G. Demailly, F. Dolhem, P. Poizot, and J.-M. Tarascon, *ChemSusChem*, 2008, **1**, 348–355.
3. A. Vlad, N. Singh, J. Rolland, S. Melinte, P. M. Ajayan, and J. F. Gohy, *Sci. Rep.*, 2014, **4**, 4315.
4. A. Vlad, J. Rolland, G. Hauffman, B. Ernould, and J.-F. Gohy, *ChemSusChem*, 2015, 10.1002/cssc.201500246.
5. S. Wang, L. Wang, Z. Zhu, Z. Hu, Q. Zhao, and J. Chen, *Angew. Chem. Intl Ed.*, 2014, **53**, 5892–5896.
6. S. Gottis, A.-L. Barrès, F. Dolhem, and P. Poizot, *ACS Appl.*

Mater. Interfac., 2014, **6**, 10870–10876.

7. H. Sano, H. Senoh, M. Yao, H. Sakaebe, and T. Kiyobayashi, *Chem. Lett.*, 2012, **41**, 1594–1596.
8. C. K. Song, B. J. Eckstein, T. L. D. Tam, L. Trahey, and T. J. Marks, *ACS Appl. Mater. Interfac.*, 2014, **6**, 19347–19354.
9. T. Yokoji, H. Matsubara, and M. Satoh, *J. Mater Chem A*, 2014, **2**, 19347–19354.
10. T. Kawai, K. Oyaizu, and H. Nishide, *Macromol.*, 2015, 10.1021/ma502396r.
11. Y. Liang, Z. Tao, and J. Chen, *Adv. Energy Mater.*, 2012, **2**, 742–769.
12. Z. Song and H. Zhou, *Energy Environ. Sci.*, 2013, **6**, 2280.
13. B. Häupler, A. Wild, and U. S. Schubert, *Adv. Energy Mater.*, 2015, 10.1002/aenm.201402034.
14. P. Novak, K. Muller, K. Santhanam, and O. Haas, *Chem. Rev.*, 1997, **97**, 207–281.
15. W. Huang, Z. Zhu, L. Wang, S. Wang, H. Li, Z. Tao, J. Shi, L. Guan, and J. Chen, *Angew. Chem. Intl. Ed.*, 2013, **52**, 9162–9166.
16. M. Lécuyer, J. Gaubicher, A.-L. Barrès, F. Dolhem, M. Deschamps, D. Guyomard, and P. Poizot, *Electrochem. Comm.*, 2015, **55**, 22–25.
17. D. Komatsu, T. Tomai, and I. Honma, *J. Pow. Sources*, 2015, **274**, 412–416.
18. Z. Song, T. Xu, M. L. Gordin, Y.-B. Jiang, I.-T. Bae, Q. Xiao, H. Zhan, J. Liu, and D. Wang, *Nano Lett.*, 2012, **12**, 2205–2211.
19. G. de Combarieu, M. Morcrette, F. Millange, N. Guillou, J. Cabana, C. P. Grey, I. Margiolaki, G. Férey, and J.-M. Tarascon, *Chem. Mater.*, 2009, **21**, 1602–1611.
20. K. Pirnat, R. Dominko, R. Cerc-Korosek, G. Mali, B. Genorio, and M. Gaberscek, *J. Pow. Sources*, 2012, **199**, 308–314.
21. C. Karlsson, H. Huang, M. Stromme, A. Gogoll, and M. Sjödin, *J. Phys. Chem. C*, 2014, **118**, 23499–23508.
22. P. Hodge and J. E. Gautrot, *Polym Int*, 2009, **58**, 261–266.
23. T. Yamamoto, T. Kimura, and K. Shiraishi, *Macromol.*, 1999, **32**, 8886–8896.
24. B. Häupler, T. Hagemann, C. Friebe, A. Wild, and U. S. Schubert, *ACS Appl. Mater. Interfac*, 2015, **7**, 3473–3479.
25. J. S. Foos, S. M. Erker, and L. M. Rembetsy, *J. Electrochem. Soc.*, 1986, **133**, 836.
26. T. Le Gall, K. H. Reiman, M. C. Grossel, and J. R. Owen, *J. Pow. Sources*, 2003, **119-121**, 316–320.
27. Z. Song, Y. Qian, X. Liu, T. Zhang, Y. Zhu, H. Yu, M. Otani, and H. Zhou, *Energy Environ. Sci.*, 2014, **7**, 4077–4086.
28. M. Morita, H. Takase, M. Ishikawa, and Y. Matsuda, *Bull. Chem. Soc. Jpn.*, 1995, **68**, 2207–2213.
29. M. Sun, W. Wang, B. He, M. Sun, W. Liu, H. Ge, Q. Zhang, and F. Sun, *J. Appl. Polym. Sci.*, 2013, **127**, 4672–4680.
30. D. Häringer, P. Novák, O. Haas, B. Piro, and M.-C. Pham, *J. Electrochem. Soc.*, 1999, **146**, 2393.
31. Y. Liang, Z. Chen, Y. Jing, Y. Rong, A. Facchetti, and Y. Yao, *J. Am. Chem. Soc.*, 2015, 10.1021/jacs.5b02290.
32. C. Karlsson, H. Huang, M. Stromme, A. Gogoll, and M. Sjödin, *J. Electroanal. Chem.*, 2014, **735**, 95–98.
33. S. Palaniappan, Y.-T. Chang, C.-M. Liu, and P. Manisankar, *J. Appl. Polym. Sci.*, 2011, **124**, 4281–4288.
34. C. Pasquini, A. Coniglio, and M. Bassetti, *Tetrahedron Lett*, 2012, **53**, 6191–6194.
35. A. Vlad, C. A. Dutu, P. Guillet, P. Jedrasik, C.-A. Fustin, U. Södervall, J.-F. Gohy, and S. Melinte, *Nano Lett.*, 2009, **9**, 2838–2843.
36. S. Renault, S. Gottis, A.-L. Barrès, M. Courty, O. Chauvet, F. Dolhem, and P. Poizot, *Energy Environ. Sci.*, 2013, **6**, 2124.
37. H. Kim, D.-H. Seo, G. Yoon, W. A. Goddard III, Y.-S. Lee, W.-S. Yoon, and K. Kang, *J. Phys. Chem. Lett.*, 2014, 3086–3092.

TOC Graphical Abstract
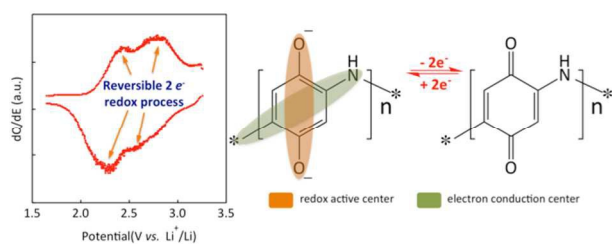
TOC Abstract: A π-conjugated redox polymer is developed and shown to hold potential towards the development of organic mixed ion- and electron-conducting materials for high-energy batteries.